magnetochemistry

MDPI

Article

Microstructure and Magnetic Property Evolution Induced by Heat Treatment in Fe-Si/SiO_2 Soft Magnetic Composites

Shaogang Li, Nachuan Ju, Jinyang Wang, Rongyu Zou, Shaochuan Lin and Minghui Yang *

Key Laboratory of Green Fabrication and Surface Technology of Advanced Metal Materials, Anhui University of Technology, Ministry of Education, Ma'anshan 243002, China; ahutlsg@163.com (S.L.); jnc18655564069@163.com (N.J.); mm55545164@163.com (R.Z.); chaim_lsc@163.com (S.L.)
* Correspondence: 19810763904@163.com

Abstract: SiO_2 has been extensively studied as a superior insulating layer for innovative Fe-based soft magnetic composites (SMCs). During the preparation process of SMCs, appropriate heat treatment can effectively alleviate internal stress, reduce dislocation density, decrease coercivity, and enhance permeability. Maintaining the uniformity and integrity of SiO_2 insulating layers during heat treatment is a challenging task. Hence, it is crucial to explore the heat-treatment process and its effects on the magnetic properties of SMCs and their insulating layers. Herein, Fe–Si/SiO_2 particles were prepared using chemical vapor deposition (CVD), and Fe–Si/SiO_2 SMCs having a core–shell heterostructure were synthesized through hot-press sintering, and investigations were conducted into how heat-treatment temperature affected the microstructure of SMCs. This study thoroughly investigated the relationship between the evolution of SiO_2 insulating layers and the magnetic properties. Additionally, the impact of the heat-treatment time on the magnetic properties of Fe-Si/SiO_2 SMCs was evaluated. The results showed that in the temperature range of 823–923 K, the core–shell heterostructures grew more homogeneous and uniform. Concurrently, the stress and defects inside the Fe-Si/SiO_2 SMCs were eliminated. When the temperature was raised over 973 K, the core–shell heterostructure was disrupted, and SiO_2 began to disperse. After following a heat-treatment process (923 K) lasting up to 60 min, the resulting SMCs had high resistivity (1.04 mΩ·cm), the lowest hysteresis loss ($P_{10\ mt/100\ kHz}$ of 344.3 kW/m^3), high saturation magnetization (191.2 emu/g). This study presents a new technique for producing SMCs using ceramic oxide as insulating layers. This study also includes a comprehensive analysis of the relationship between microstructure, magnetic properties, and heat treatment process parameters. These findings are crucial in expanding the potential applications of ceramic oxide.

Keywords: ceramic oxide; insulating layer; soft magnetic composites; heat treatment; microscopic change; magnetic properties

Citation: Li, S.; Ju, N.; Wang, J.; Zou, R.; Lin, S.; Yang, M. Microstructure and Magnetic Property Evolution Induced by Heat Treatment in Fe-Si/SiO_2 Soft Magnetic Composites. *Magnetochemistry* **2023**, *9*, 169. https://doi.org/10.3390/magnetochemistry9070169

Academic Editor: Krzysztof Chwastek

Received: 17 May 2023
Revised: 22 June 2023
Accepted: 27 June 2023
Published: 29 June 2023

1. Introduction

Soft magnetic composites (SMCs), which have high saturation magnetization, high permeability, and relatively low core loss, have been regarded as key components of electromagnetic systems in higher-frequency ranges [1]. The advancement in frequency conversion control techniques has made it imperative to minimize energy conversion loss in SMCs in order to achieve the miniaturization and high-efficiency application of high-frequency devices. SMCs are typically made up of iron or iron-based soft magnetic particles that are coated with a thin insulating layer to form a core–shell heterostructure using either physical or chemical methods. These particles are then compressed into the desired shape and heat-treated. Soft magnetic particle matrix construction maintains excellent magnetic properties, while the insulating layer significantly reduces eddy current loss in SMCs. Heat-treatment conditions are crucial in SMC design and development [2]. High internal stress and defect density, particularly dislocations, increase hysteresis loss during

the compaction process. However, appropriate heat-treatment conditions can effectively reduce dislocation density, coercivity, and hysteresis loss while enhancing permeability in SMCs.

In recent times, there has been a surge in interest toward inorganic ceramic materials, such as SiO_2 [3], Al_2O_3 [4], and ZrO_2 [5], owing to their exceptional all-around properties. These materials are easily obtainable, cost-effective, and environmentally friendly. Compared to traditional organic insulating materials, inorganic ceramic materials possess several advantages such as high resistivity, exceptional thermal stability, and chemical stability [6]. Previously, SMCs exhibiting desirable magnetic properties were created through the use of a SiO_2 insulating layer via the CVD method. The evolution process of the core–shell heterostructure was examined during high-temperature sintering. A study found that ceramic insulating layers have high hardness and brittleness, which causes them to shatter easily at high temperatures [7]. This leads to damage to the core–shell heterostructure, which hinders the reduction in eddy current loss in SMCs. In order to improve magnetic performance and broaden the application range of SMCs with inorganic ceramic insulating layers, it is important to develop techniques to customize the heat-treatment mechanism. Tian utilized the sol–gel method to successfully design and manufacture FeSiBNbCu/SiO_2 SMCs [2], while also thoroughly evaluating how the temperature of the heat-treatment process affected the soft magnetic properties. Lei et al. [8] achieved outstanding magnetic properties by heating iron-based SMCs with an Al_2O_3 insulating layer at 573–773 K for 60 min under an Ar atmosphere. However, when annealed at 873 K, the magnetic properties of the SMCs were dramatically weakened as a result of the interaction between the decomposition product of zinc stearate and the Al_2O_3 insulating layer. Li et al. [9] synthesized Fe–Si–Al-based SMCs with an ultrathin MoO_3 composite insulating layer using a two-step heat-treatment process and evaluated how their magnetic and mechanical properties and electrical resistivity were affected by the initial and subsequent steps of heat-treatment temperatures. The magnetic properties of SMCs were enhanced through modifications in heat-treatment parameters. However, there are only a few published studies on the impact of heat treatment on the evolution of the core–shell heterostructure and magnetic properties of SMCs. A better understanding of these aspects can contribute to the improvement of SMC design.

This study investigates the effect of heat-treatment parameters on the microscopic changes in and magnetic properties of Fe–Si/SiO_2 SMCs, which were synthesized using CVD and hot-press sintering [10]. A comprehensive study was undertaken to explore the correlation between the magnetic characteristics and structure of SMCs. The effect of varying heat-treatment durations was also examined in relation to the magnetic properties of Fe-Si/SiO_2 SMCs.

2. Experimental Procedure

The powdered Fe–Si alloys were sourced from Hualiu New Materials Co., Ltd. The powders had a composition of Fe (93.4 wt%) and Si (6.6 wt%), with an average particle diameter of 50 μm, and were produced via gas atomization. Tetraethyl orthosilicate ($C_8H_{20}O_4Si$, 99.0%) was purchased from Zhiyuan Chemical Reagent Co., Ltd. (Shenzhen, China). Finally, Tianze Gas Co., Ltd. (Nanjing, China) provided Ar gas (99.99%).

Fe-Si/SiO_2 powders were synthesized through the CVD method (Figure 1), with Fe-Si as the core and silicon dioxide as the shell. The process involved placing the Fe-Si powder on a mesh sieve with 30 μm wide holes in a vertical tube oven and fluidizing it with argon. To synthesize the core–shell particles, tetraethyl orthosilicate was inserted into the oven at 667 °C under a constant argon flow of 300 mL/min for 60 min. The resulting mixture was then placed in a graphite die containing 28.0 g of the particles and sintered in a furnace with pressure assistance (14 MPa). The sintering process was conducted in a temperature range of 298–1153 K. The temperature was gradually increased over a period of 600 s and then maintained at 1153 K for 600 s. Then, the cooling rate was 1 K/s until 323 K. The obtained SMCs were heat-treated at 823, 873, 923, 973, and 1023 K for 30, 60,

90, and 120 min after sintering, and the obtained SMCs' ultimate measurements were as follows: the as-synthesized SMCs had dimensions of 30 mm in outer diameter, 20 mm in inner diameter, and 5 mm in height. To examine their characteristics, XRD with Cu Kα radiation (Bruker D8 Advance, Saarbrucken, Germany) was used to analyze the solid-state structure, while SEM (Tescan MIRA3 XMU, Brno, Czech Republic) was used to analyze the morphologies and local chemical homogeneities. The magnetic characteristics of the SMCs were examined under normal industrial settings using a B-H curve analyzer (SY-8258 IWATSU, Tokyo, Japan). At 298 K, a vibrating sample magnetometer (MPMS-3) was employed to investigate hysteresis loops over a magnetic field range of ± 20,000 Oe, with a step size of 50 Oe. The resistivity of SMCs was measured using a ST2253y (Suzhou lattice Electronics Co., Ltd, Suzhou, China) resistivity tester.

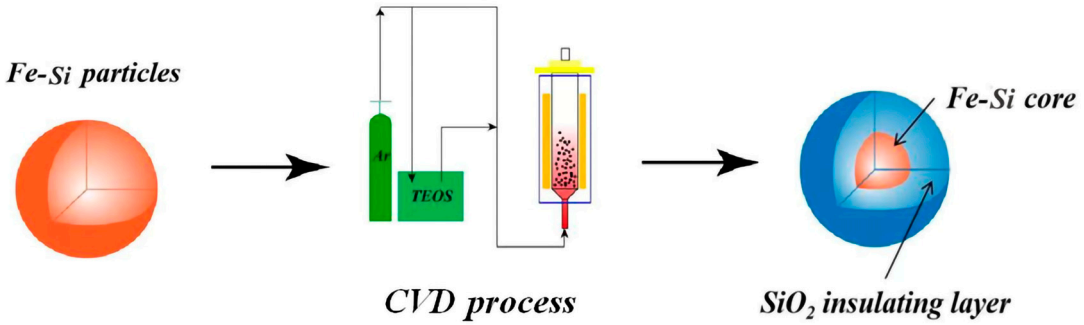

Figure 1. Fe-Si/SiO_2 powder was synthesized by CVD method.

3. Results and Discussion

3.1. Evolution of the Core–Shell Heterostructure within the Fe–Si/SiO_2 SMCs

Figure 2a–f presents the refined backscattered electron images (BSEs) of the Fe-Si/SiO_2 SMCs after heat treatment at different temperatures. The images clearly show that the number of pores in the heat-treated Fe–Si/SiO_2 SMCs samples was lower than that in the SMCs samples without heat treatment, as depicted in Figure 2a. The study revealed that with an increase in the heat-treatment temperature from 823 K to 923 K, the size of pores decreased considerably, as shown in Figure 2b–d. This was due to the even distribution of the coatings and the subsequent increase in density and decrease in porosity with the rising heat-treatment temperature. The SiO_2 coating was progressively distributed along the edge of the Fe-Si particles and became denser. The core–shell structure was fully preserved until 923 K. However, at 973 K, black spots began to form at the Fe-Si particle boundaries, indicating overheating (Figure 2e) [11]. After increasing the heat-treatment temperature to 1023 K, as shown in Figure 2f, the previously organized grey zone began to exhibit black pots, indicating that SiO_2 was no longer confined to the edge of the particles but was instead dispersing, leading to the disruption of the core–shell heterostructure. This can be attributed to the excessive heat-treatment temperature [12], which leads to the deformation of Fe-Si particles and the detachment of the insulating layer.

The X-ray diffraction (XRD) patterns of Fe-Si/SiO_2 SMCs, before and after heat treatment at 923 K, are presented in Figure 3. Three diffraction peaks can be observed at 44.32°, 64.75°, and 82.36°, which correspond to the (110), (200), and (211) planes, respectively, of the body-centered cubic structure's -Fe(Si) (COD 96-900-6622) phase. The crystal's space group is Im3m (229) and exhibits characteristic peaks at 41.79° and 48.76°, indicating the presence of the SiO_2 phase (COD 96-901-2604). The XRD experimental results were refined using Rietveld refinement to estimate potential phase changes in the Fe-Si/SiO_2 SMCs. The Rietveld calculations were found to be consistent with the experimental results based on the low values of R_p (peak residual variance factor), which were 7.22 before heat treatment and 7.18 after heat treatment, and S (goodness of fit), which were 1.96 before heat treatment and 1.58 after heat treatment. Meanwhile, the unit cell parameters before and after heat treatment were almost unchanged (for α-Fe (Si)—a = b = c = 2.849, α = β = γ = 90°; for

SiO_2—a = b = 4.625, c = 5.216, α = β = 90°, γ = 120°). This indicates that the heat treatment had a slight to no effect on the Fe-Si/SiO_2 SMCs' internal structure.

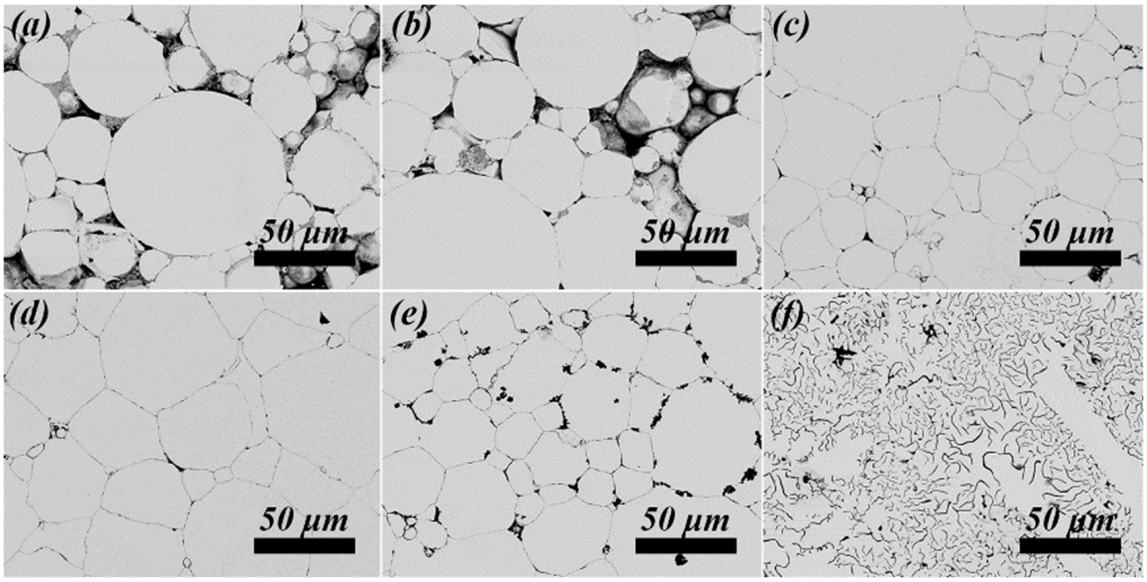

Figure 2. Fe-Si/SiO_2 SMCs' polished surfaces in backscattered electron images before (**a**) and after heat treatment at 823 (**b**), 873 (**c**), 923 (**d**), 973 (**e**), and 1023 (**f**) K.

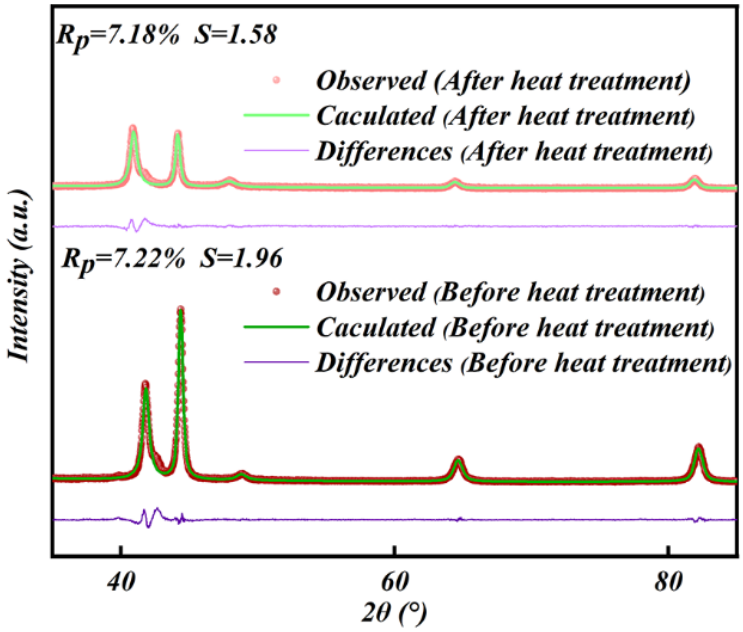

Figure 3. Fe-Si/SiO_2 SMCs' X-ray diffraction patterns before and after heat treatment.

3.2. Effects of Heat-Treatment Temperature on the Magnetic Properties of Fe–Si/SiO_2 SMCs

Figure 4 illustrates the magnetic hysteresis loops of the Fe-Si/SiO_2 soft magnetic composites (SMCs) after undergoing heat treatment. The saturation magnetization (Ms) of the heat-treated Fe-Si/SiO_2 SMCs is significantly higher than that of the non-treated SMCs. As the heat-treatment temperature increases from 823 K to 1023 K, the Ms values also increase considerably, as shown in Figure 4a. This is due to the increase in density observed in the SEM topography of the Fe-Si/SiO_2 SMC surface after polishing (Figure 2), which leads to a higher content of magnetic particles in the unit volume of Fe-Si/SiO_2 SMCs. Furthermore, despite the destruction of the core–shell structure, the phase composition

remains almost unchanged, suggesting that the heat treatment did not affect the number of magnetic phases. According to the magnetization theory, the relationship between coercivity and the magnetic anisotropy constant, saturation magnetostriction coefficient, internal stress, and saturation magnetization of soft magnetic materials is

$$H_c \propto (\lambda_s \sigma + K)/Ms^2 \quad (1)$$

where λ_s is the saturation magnetostriction coefficient, *Ms* is the saturation magnetization, σ is the internal stress, and K is the magnetic anisotropy constant. The increase in the heat-treatment temperature not only reduced the internal stress but also increased the saturation magnetization. Therefore, it can be seen from Equation (1) that the coercive force gradually decreases. Additionally, elevated heat-treatment temperatures may lead to grain growth [13–15], subsequently causing a reduction in grain boundary density [16]. This, in turn, results in a decrease in coercivity due to a decrease in the effect of fixing the domain walls. As the heat-treatment temperature increases, it creates an excessive temperature field within the powder. This field gradually decreases from the inside out, leading to a change in the size and shape of the Fe-Si particles. This constrains the expansion or contraction of the adjacent area and generates new internal stress [17]. Therefore, the coercivity increases again, as shown in Figure 4b.

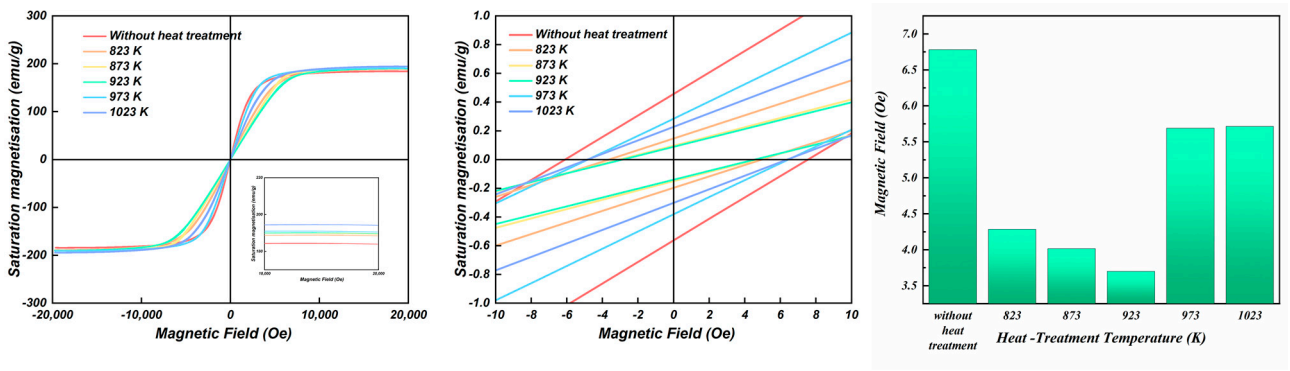

(**a**) (**b**) (**c**)

Figure 4. Fe-Si/SiO_2 SMCs' saturation magnetization and coercivity (**a**,**b**); coercivity (**c**) at different heat treatment temperatures.

Resistivity, which is inversely proportional to conductivity, is a useful parameter for characterizing the electrical conduction of metal composites. The presence of defects in conduction electrons acts as scattering centers, and reducing these defects can lead to a decrease in resistivity [18] as the heat-treatment temperature increases. The disappearance of pores generated during the molding process also contributes to this trend [7]. Even though the SiO_2 insulating layers become more complete and uniform on the surface of the Fe–Si particles as the internal stress decreases, as shown in Figure 5, the resistivity still slightly decreases within the 823–973 K range for the heat treatment. Moreover, the downward trend may be impacted by the increased grain size of the Fe-Si/SiO_2 SMCs with higher heat-treatment temperatures while the density of the grain boundary with the higher resistivity decreases [19]. As the temperature of the heat treatment increased, the Fe-Si particles underwent deformation and the SiO_2 particles were dispersed throughout the material rather than being confined to the surface of the particles. This dispersion occurred due to damage to the core–shell structure and the prevention of the initial separation of the Fe-Si particles [20]. As a result, the resistivity of the material was significantly reduced.

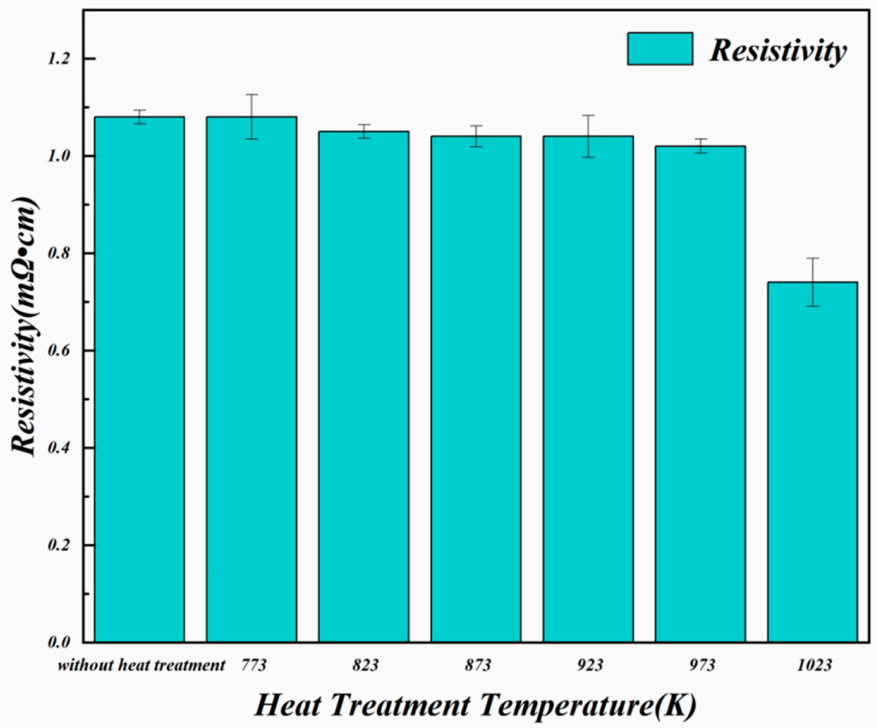

Figure 5. The resistivity of Fe-Si/SiO_2 SMCs following heat treatment.

Figure 6 illustrates the impact of temperature variations on the frequency stability and permeability of the SMC. Generally, with increasing working frequency, the Fe–Si/SiO_2 SMCs' permeability decreases [21]. The domain walls become harder to move as a result of the residual stress's impact on the magnetic properties of SMCs, and the pinning effect that results in lower permeability [22]. As a consensus, high-temperature heat treatment can reduce dislocation density, produce defects with a low-volume proportion, and remove residual stress [23,24]. However, at higher frequencies, the decreased permeability is caused by the magnetic dilution effect in complete and dense insulating layers. As a consequence, the resistivity is increased because the Fe-Si particles are prevented from interacting. Another explanation for this is SiO_2 and Fe-Si particles were exchange-coupled, resulting in an efficient surface spin orientation [25]. Nevertheless, after heat treatment at higher temperatures, the permeability of the Fe-Si/SiO_2 SMCs stabilizes at higher frequencies because a complete insulating layer favors an increase in the depth of the skin effect as the working frequency rises [26]. As the temperature for heat treatment increased to 973 and 1023 K, it caused the powders' substrate to come into close contact with the breakdown of the core–shell heterostructure, leading to a faster decline in permeability. However, when SMCs were heat-treated at 923 K, it resulted in a higher and more stable magnetic permeability that was maintained across a wider frequency range.

The distribution of various types of Fe-Si/SiO_2 SMCs' total loss (P_{cv}) is shown in Figure 7a. The P_{cv} values increased with frequency for all SMCs. Additionally, P_{cv} initially increased with higher heat-treatment temperatures before decreasing. The SMCs heat treated at 923 K had the lowest total loss, reaching 639.9 kW/m^3, which was a 32.6% and 27.8% decrease compared to SMCs that underwent heat treatment at 1023 K and those that did not.

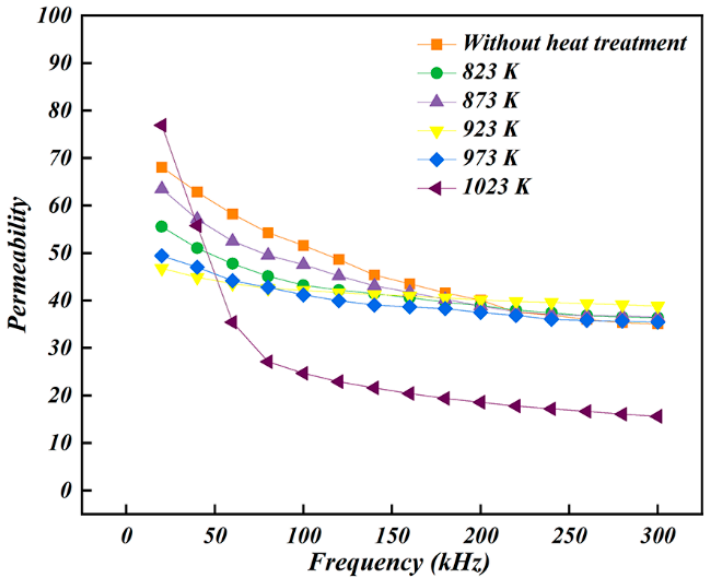

Figure 6. Permeability of the various types of Fe–Si/SiO_2 SMCs.

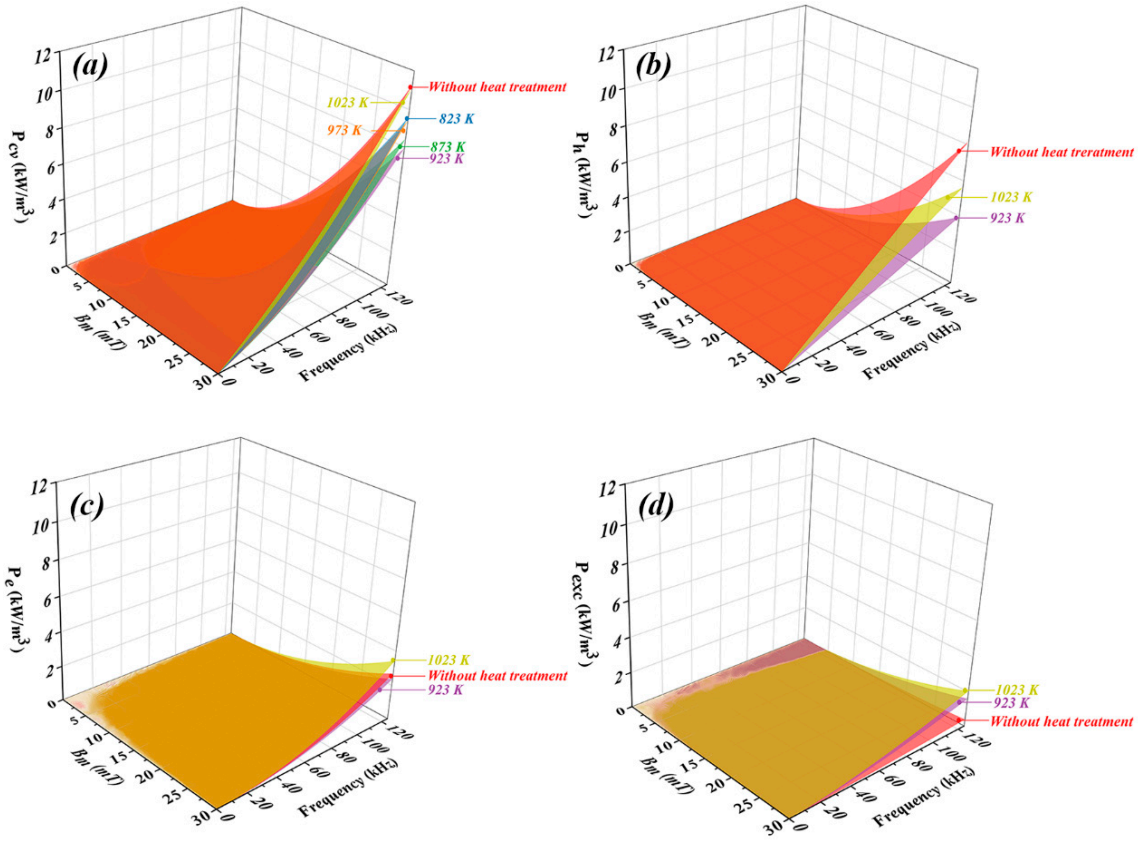

Figure 7. Total loss (**a**), hysteresis loss (**b**), eddy current loss (**c**), and excess loss (**d**) of the SMCs after heat treatment at various temperatures.

As per the classical Bertotti loss separation theory [20], P_{cv} can be split into three parts: hysteresis loss (P_{hyst}), eddy current loss (P_e), and excess loss (P_{exc}) [27].

$$P_{cv} = P_{hyst} + P_{ec} + P_{exc} \quad (2)$$

The area of the quasi-static hysteresis loop multiplied by the frequency is the definition of P_{hyst}, as in Equation (3) below:

$$P_{hyst} = C_{hyst} B_m^{\alpha} f \tag{3}$$

where f is the frequency; B_m is the maximum induction; C_{hyst}, as the simulation factor, is the hysteresis coefficient; and α, for the majority of ferromagnetic materials and alloys, ranges between 1.6 and 2.2. P_{ec}, depending on the efficiency of vortex operation, and can be defined as:

$$\begin{aligned} P_{ec} &= P_{ec}^{inter} + P_{ec}^{intra} \\ &= 6\pi^2 d_{eff}^2 \times B_m^2 f^2 [-0.633 \times (w/h)\tanh(1.58h/w) + 1]^{-1} \beta_1 \rho_s + \pi^2 d^2 \times B_m^2 f^2 \left(\beta_2 \rho_p\right)^{-1} \end{aligned} \tag{4}$$

where P_{ec}^{inter} and P_{ec}^{intra} are the inter- and intra-particle eddy current coefficients, respectively. The effective eddy current dimension thickness is the specimen (d_{eff}), and the particle size is d. ρ_s and ρ_p stand for the specimen's and the particles' bulk resistivity, respectively. w and h stand for the rectangle's width and height, respectively, whereas β_1 denotes the geometrical property of the rectangle's cross-section. Different geometries have different values for the granular geometrical constant β_2; for spheres, β_2 = 20 [1]. Pexc depends on the test frequency, applied magnetic field, and the number of active magnets in quasi-static and dynamic magnetization. Therefore, $P_{exc} \propto f^{1.5}$ is not accurate enough to analyze the loss separation. The expression is changed as follows:

$$P_{exc} = C_{exc} B_m^x f^y \tag{5}$$

The coefficients for the magnetic field and frequency are x and y, respectively, where C_{exc} is the excess coefficient. Initially, the P_{cm}/f vs. f curve was fit using a linear fitting method, and the fitted curve was extrapolated to the zero-frequency point to obtain the intercept of the hysteresis loss value under quasi-static conditions. By nonlinear fitting of quasi-static P_{hyst} at different magnetic field intensities, C_{hyst} and α can be obtained. Then, based on Equation (5) [28], the eddy current loss parameters obtained in Equation (4) and the hysteresis loss parameters are combined to calculate the constants of the residual loss, as shown in Table S1. By separating the loss of various SMCs, the influence of heat-treatment temperature on the loss of SMCs' core–shell structure and SiO_2 insulating layers was further understood, as can be seen in Figure 7b–d.

At lower heat-treatment temperatures, the residual stress in SMCs remains unreleased, resulting in a higher P_{hyst}. However, as the heat-treatment temperature increases, lattice defects decrease, tension is released, and the magnetic domain structure relaxes, leading to a decline in P_{hyst}. The grain size also plays a crucial role in affecting P_{hyst}, as smaller grain sizes result in higher grain boundary density, which ultimately fixes domain walls and significantly impacts P_{hyst}. A rise in heat-treatment temperature is frequently accompanied by an increase in grain size. As a result, P_{hyst} initially dropped as the heat-treatment temperature rose. Regrettably, the substrate of core–shell particles is deformed by the high heat-treatment temperature, which causes the SMCs' internal structure to revert to chaos and cause P_{hyst} to rise. The Pec value remained relatively stable in the temperature range of 823–973 K due to minimized stress during the pressing process and maintained the integrity of the insulating layers, resulting in less fluctuation compared to P_{hyst}.

As the temperature of heat treatment increased to 1023 K, the insulating layers between the ferromagnetic particles dispersed within the SMCs. This led to the formation of point contact between Fe-Si particles, causing the effective radius of the eddy current to expand and resistivity to drop. As a result, P_{ec} increased. Compared to SMCs without heat treatment, only 11.8% less P_{ec} was lost in the SMCs heat treated at 923 K, whereas the P_{hyst} decreased by 41.9%. And, hence, the strongest effect of heat treatment temperature on loss was P_{hyst}. Table 1 lists SMCs' magnetic properties wherein, clearly, 923 K and 973 K are the preferable temperatures for heat treatment.

Table 1. Comparison of magnetic properties of SMCs with different heat-treatment temperatures.

Heat-Treatment Temperature (K)	Permeability (300 kHz)	Saturation Magnetization (emu/g)	Coercivity (Oe)	Resistivity (mΩ·cm)	Total Loss at 10 mT and 100 kHz (kW/m^3)
Before heat treatment	40.5	184.0	7.6	1.08	1131.3
823	37.7	188.9	5.1	1.05	949.3
873	38.5	189.8	5.0	1.04	867.1
923	39.4	191.2	4.9	1.04	779.3
973	38.8	190.9	6.3	1.02	710.0
1023	15.8	194.5	6.4	0.74	1043.4

3.3. Effects of Heat-Treatment Time on the Magnetic Properties of Fe–Si/SiO_2 SMCs

Table 2 displays the magnetic properties of the Fe-Si/SiO_2 SMCs that were heat-treated at 923 K for different durations. The purpose of this analysis was to investigate the effect of heat-treatment time on magnetic properties. Figure 8 illustrates the microstructure and evolution of SMCs, along with their magnetic properties, including saturation magnetization, coercivity, permeability, resistivity, and hysteresis loss. According to Figure 8 and Table 2, the saturation magnetization increases as the heat-treatment time is extended, while the SMCs gradually become denser. Additionally, the coercivity decreases as stress and defects are relieved, but increases with the presence of a chaotic internal magnetic domain structure and a destroyed core–shell heterostructure. Hysteresis loss has a similar trend and permeability exhibits the opposite. It is significantly different for resistivity; it slightly decreases owing to the reduction in pores with the extension of the heat-treatment time, and a significant drop occurs after the Fe–Si particles are deformed under an excessively long heat-treatment time, which destroys the core–shell heterostructure.

Table 2. Comparison of magnetic properties of SMCs heat-treated at various times.

Heat-Treatment Time (min)	Permeability (300 kHz)	Saturation Magnetization (emu/g)	Coercivity (Oe)	Resistivity (mΩ·cm)	Hysteresis Loss at 10 mT and 100 kHz (kW/m^3)
Before heat treatment	35.1	184.0	7.6	1.08	821.2
30	36.1	190.4	5.9	1.04	626.5
60	39.4	191.2	4.9	1.04	344.3
90	36.5	193.9	5.1	1.03	489.2
120	12.1	195.3	8.3	0.85	520.6

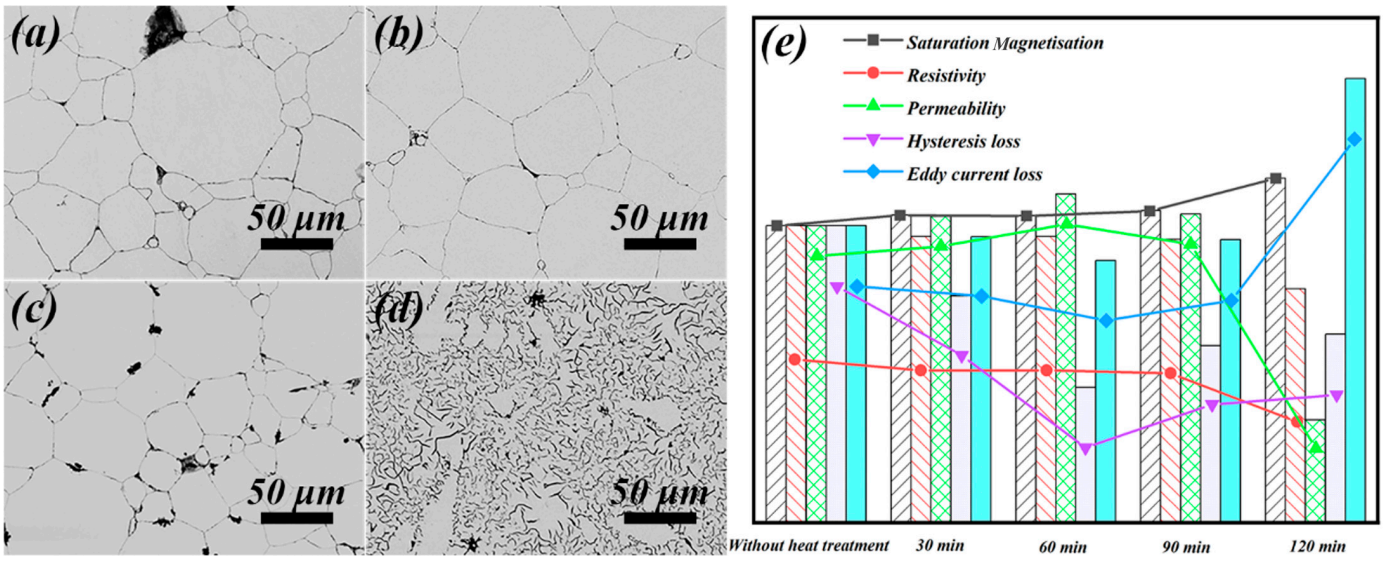

Figure 8. Backscattered electron images of the polished surfaces of the SMCs heat-treated at different times: (**a**) 30 min, (**b**) 60 min, (**c**) 90 min, (**d**) 120 min, and magnetic properties (**e**) of the SMCs heat-treated at different times.

These results suggest that a shorter heat-treatment time has a limited effect on the removal of stress, as defects still persist in the particles. This, in turn, hinders the improvement in permeability and reduction in hysteresis loss. On the other hand, an excessive heat-treatment time can lead to the destruction of the insulating layer, which significantly decreases resistivity and increases eddy current loss. Therefore, the ideal heat-treatment time at a temperature of 923 K was found to be between 60 and 90 min.

4. Conclusions

This study aimed to analyze the magnetic properties of Fe-Si/SiO_2 SMCs and the effect of heat-treatment parameters on the microscopic characteristics of core–shell heterostructures. The main findings can be summarized as follows:

Firstly, the study found that as the heat-treatment temperature increased within a range of 823–923 K, the core–shell heterostructures became more uniform and the SiO_2 insulating layers became more homogeneous. At the same time, the stress and defects inside the SMCs were gradually eliminated. The core–shell heterostructure of the SMCs was found to be damaged when the heat-treatment temperature exceeded 973 K, causing SiO_2 to scatter. In addition, increasing the heat-treatment temperature resulted in a decrease in resistivity, coercivity, and total loss (primarily, hysteresis loss). However, the loss and coercivity increased again when the heat-treatment temperature exceeded 973 K. The resistivity gradually decreased due to the damaged core–shell heterostructure, while the saturation magnetization remained relatively stable. Similar results were obtained for the impact of the heat-treatment time on magnetic properties. Comparing the magnetic properties, it was concluded that a heat-treatment time of 60–90 min was most appropriate. Finally, when the SMCs were heat-treated at 923 K for 60 min, they showed stabilization of permeability at lower frequencies and exhibited a relatively low hysteresis loss ($P_{hyst,10\ mT\ and\ 100\ kHz}$ of 344.3 kW/m^3) with a 41.9% reduction, a *Ms* of 191.2 emu/g, and a resistivity of 1.04 mΩ·cm, which owns the best magnetic properties. This study provides a novel method for fabricating SMCs with ceramic oxide as the insulating layers and a thorough analysis of the interactions between the microstructure, magnetic properties, and heat-treatment process parameters. These findings are essential for extending the range of applications for ceramic oxide.

Supplementary Materials: The following supporting information can be downloaded at: https://www.mdpi.com/article/10.3390/magnetochemistry9070169/s1, Table S1: C_{hyst}, C_{ec}, C_{exc} and other fitting parameters of the SMCs heat-treated at various temperatures.

Author Contributions: S.L. (Shaogang Li), writing—original draft, formal analysis, and investigation; N.J., picture rendering and review; J.W., performance test, investigation, and methodology; S.L. (Shaochuan Lin) and R.Z., project administration; M.Y., review, editing, and project administration. All authors have read and agreed to the published version of the manuscript.

Funding: This work was supported by the Chinese National Science Foundation (52274311), Scientific Research Planning Project of Anhui Province (2022AH040054, 2022AH010024), and Key Research and Development Plan of Anhui Province (202104b11020007).

Institutional Review Board Statement: Not applicable.

Informed Consent Statement: Not applicable.

Data Availability Statement: Not applicable.

Acknowledgments: The authors would like to thank Zhaoyang Wu and Rui Wang from Anhui University of Technology for fruitful guidance.

Conflicts of Interest: The authors declare that they have no known competing financial interests or personal relationships that could have appeared to influence the work reported in this paper.

References

1. Li, W.; Cai, H.; Kang, Y.; Ying, Y.; Yu, J.; Zheng, J.; Qiao, L.; Jiang, Y.; Che, S. High permeability and low loss bioinspired soft magnetic composites with nacre-like structure for high frequency applications. *Acta Mater.* **2019**, *167*, 267–274. [CrossRef]
2. Tian, M.; Xu, J.; Yang, S.; Wang, J.; Yang, T.; Li, G.; Chen, Q.; Liu, X. Effects of heat treatment and compaction pressure on the microstructure and magnetic properties of core-shell structured FeSiBNbCu/SiO_2 soft magnetic composites. *J. Alloys Compd.* **2022**, *923*, 166394. [CrossRef]
3. Wu, C.; Huang, M.; Luo, D.; Jiang, Y.; Yan, M. SiO_2 nanoparticles enhanced silicone resin as the matrix for Fe soft magnetic composites with improved magnetic, mechanical and thermal properties. *J. Alloys Compd.* **2018**, *741*, 35–43. [CrossRef]
4. Peng, Y.; Yi, Y.; Li, L.; Yi, J.; Nie, J.; Bao, C. Iron-based soft magnetic composites with Al2O3 insulation coating produced using sol–gel method. *Mater. Des.* **2016**, *109*, 390–395. [CrossRef]
5. Geng, K.; Xie, Y.; Xu, L.; Yan, B. Structure and magnetic properties of ZrO_2-coated Fe powders and Fe/ZrO2 soft magnetic com-posites. *Adv. Powder Technol.* **2017**, *28*, 2015–2022. [CrossRef]
6. Wang, R.; He, Y.; Kong, H.; Wang, J.; Wu, Z.; Wang, H. Influence of sintering temperature on heterogeneous-interface structural evolution and magnetic properties of Fe–Si soft magnetic powder cores. *Ceram. Int.* **2022**, *48*, 29854–29861. [CrossRef]
7. Rakshit, R.; Das, A.K. A review on cutting of industrial ceramic materials. *Precis. Eng.* **2019**, *59*, 90–109. [CrossRef]
8. Zheng, J.; Zheng, H.; Lei, J.; Qiao, L.; Ying, Y.; Cai, W.; Li, W.; Yu, J.; Liu, Y.; Huang, X.; et al. Structure and magnetic properties of Fe-based soft magnetic composites with an Li–Al–O insulation layer obtained by hydrothermal synthesis. *J. Alloys Compd.* **2019**, *816*, 152617. [CrossRef]
9. Li, Z.; Li, Z.; Liu, X.; Shi, S.; Li, H.; Liu, X. Ultra-low core loss FeSiAl-based soft magnetic composites with ultra-thin MoO_3 composite insulating layer. *Ceram. Int.* **2022**, *48*, 29705–29714. [CrossRef]
10. Wu, Z.; Xian, C.; Jia, J.; Liao, X.; Kong, H.; Xu, K. Formation Process of the Integrated Core (Fe-6.5wt.% Si)@Shell(SiO_2) Structure Obtained via Fluidized Bed Chemical Vapor Deposition. *Metals* **2020**, *10*, 520. [CrossRef]
11. Fan, J.; Han, Y.; Li, P.; Sun, Z.; Zhou, Q. Micro/nano composited tungsten material and its high thermal loading behavior. *J. Nucl. Mater.* **2014**, *455*, 717–723. [CrossRef]
12. Huang, X.; Ding, S.; Wang, Z.; Wang, L.; Liu, M.; Wang, Z.; Liang, X.; Liu, W. Effects of annealing temperature on the structure characteristics of Fe83Si6B6Cu1Nb1P1.5C1.5 amorphous ribbons. *J. Non-Cryst. Solids* **2022**, *580*, 121388. [CrossRef]
13. Wang, G.-Q.; Chen, M.-S.; Li, H.-B.; Lin, Y.C.; Zheng, W.-D.; Ma, Y.-Y. Methods and mechanisms for uniformly refining deformed mixed and coarse grains inside a solu-tion-treated Ni-based superalloy by two-stage heat treatment. *J. Mater. Sci. Technol.* **2021**, *77*, 47–57. [CrossRef]
14. Tan, G.-L.; Tang, D.; Dastan, D.; Jafari, A.; Silva, J.P.; Yin, X.-T. Effect of heat treatment on electrical and surface properties of tungsten oxide thin films grown by HFCVD technique. *Mater. Sci. Semicond. Process.* **2020**, *122*, 105506. [CrossRef]
15. Lee, S.-H.; Choi, J.S.; Yoon, D.Y. The Dependence of Abnormal Grain Growth on Initial Grain Size in 316 L Stainless Steel. *Int. J. Mater. Res.* **2001**, *92*, 655–662. [CrossRef]
16. Yang, H.; Wu, L.; Jiang, B.; Liu, W.; Song, J.; Huang, G.; Zhang, D.; Pan, F. Clarifying the roles of grain boundary and grain orientation on the corrosion and discharge processes of α-Mg based Mg-Li alloys for primary Mg-air batteries. *J. Mater. Sci. Technol.* **2020**, *62*, 128–138. [CrossRef]
17. Ahmed, N.M.; Sabah, F.A.; Abdulgafour, H.; Alsadig, A.; Sulieman, A.; Alkhoaryef, M. The effect of post annealing temperature on grain size of indium-tin-oxide for optical and electrical properties improvement. *Results Phys.* **2019**, *13*, 102159. [CrossRef]
18. Shokrollahi, H.; Janghorban, K. Effect of warm compaction on the magnetic and electrical properties of Fe-based soft magnetic composites. *J. Magn. Magn. Mater.* **2007**, *313*, 182–186. [CrossRef]
19. Fulop, G.; Dias, M.; Sandim, H.; Bormio-Nunes, C. High saturation magnetic induction and low magnetostriction of a novel ferritic Fe-Ti alloy compared to a non-oriented silicon steel. *J. Magn. Magn. Mater.* **2021**, *527*, 167702. [CrossRef]
20. Bertotti, G. *Hysteresis in Magnetism: For Physicists, Materials Scientists, and Engineers*; Gulf Professional Publishing: Houston, TX, USA, 1998.
21. Huang, J.; Xu, G.; Liang, Y.; Hu, G.; Chang, P. Improving coal permeability using microwave heating technology—A review. *Fuel* **2020**, *266*, 117022. [CrossRef]
22. Landgraf, F.; Emura, M. Losses and permeability improvement by stress relieving fully processed electrical steels with previous small deformations. *J. Magn. Magn. Mater.* **2001**, *242–245*, 152–156. [CrossRef]
23. Qian, L.; Peng, J.; Xiang, Z.; Pan, Y.; Lu, W. Effect of annealing on magnetic properties of Fe/Fe3O4 soft magnetic composites prepared by in-situ oxidation and hydrogen reduction methods. *J. Alloys Compd.* **2018**, *778*, 712–720. [CrossRef]
24. Kwon, S.; Kim, S.; Yim, H.; Kang, K.H.; Yoon, C.S. High saturation magnetic flux density of Novel nanocrystalline core annealed under magnetic field. *J. Alloys Compd.* **2020**, *826*, 154136. [CrossRef]
25. Qiu, Y.; Wang, R.; He, Y.; Kong, H.; Li, S.; Wu, Z. Effects of axial pressure on the evolution of core–shell heterogeneous structures and magnetic properties of Fe–Si soft magnetic powder cores during hot-press sintering. *RSC Adv.* **2022**, *12*, 19875–19884. [CrossRef]
26. Dong, B.; Qin, W.; Su, Y.; Wang, X. Magnetic properties of FeSiCr@MgO soft magnetic composites prepared by magnesium acetate pyrolysis for high-frequency applications. *J. Magn. Magn. Mater.* **2021**, *539*, 168350. [CrossRef]

27. Kollára, A.; Olekšáková, D.; Vojtek, V.; Füzer, J.; Fáberová, M.; Bureš, R. Steinmetz law for ac mag-netized iron-phenolformaldehyde resin soft magnetic composites. *J. Magn. Magn. Mater.* **2017**, *424*, 245–250. [CrossRef]
28. Guo, Z.; Wang, J.; Chen, W.; Chen, D.; Sun, H.; Xue, Z.; Wang, C. Crystal-like microstructural Finemet/FeSi compound powder core with excellent soft magnetic properties and its loss separation analysis. *Mater. Des.* **2020**, *192*, 108769. [CrossRef]